Contribution of NOMA Signalling to Practical Multibeam Satellite Deployments

Tomás Ramírez*, Carlos Mosquera†

* Centro Tecnolóxico de Telecomunicacións de Galicia (Gradiant), Carretera do Vilar, 56-58 36214 Vigo, Spain

† atlanTTic research center, Universidade de Vigo, 36310 Vigo, Spain

Email: tramirez@gradiant.org, mosquera@gts.uvigo.es

***Abstract*—This work explores the contribution of Non-Orthogonal Multiple Access (NOMA) signalling to improve some relevant metrics of a multibeam satellite downlink. Users are paired to exploit Signal-to-Noise Ratio (SNR) imbalances coming from the coexistence of different types of terminals, and they can be flexibly allocated to the beams, thus relaxing the cell boundaries of the satellite footprint. Different practical considerations are accommodated, such as a spatially non-uniform traffic demand, non-linear amplification effects, and the use of the DVB-S2X air interface. Results show how higher traffic volumes can be channelized by the satellite, thanks to the additional bit rates which are generated for the strong users under the superposition of signals, with carefully designed power levels for DVB-S2X modulation and coding schemes in the presence of non-linear impairments.**

I. Introduction

Very promising non-orthogonal transmission schemes with interference cancellation at the receivers have appeared in the last decade, with high potential to exploit multi-user interference. This is the case of the so-called non-orthogonal multiple access (NOMA) scheme, presented in [1] and, in particular, its power domain version, PD-NOMA, which is known to be information theoretically optimal in the sense that it maximizes the achievable rate region for single-antenna transceivers [2]. The ultimate goal is to improve the performance of conventional orthogonal multiple access (OMA), such as FDMA or TDMA. In fact, the growth of the achievable rate region of NOMA with respect to OMA increases with the gap in the received Signal-to-Noise Ratio (SNR) among users. In the case of satellite scenarios, the application of NOMA has been discussed in several works under different assumptions, see, e.g., [3], [4], or [5], among others, and also the use of more general techniques such as Rate Splitting, more appropriate when several antennas can collaborate to serve several users under the linear precoding of the different transmit symbols [6], [7].

Taking into account that PD-NOMA can play a major role when serving several users with the same antenna, in particular if the channel quality varies significantly across users, we address a satellite system scenario with a frequency reuse scheme such that the co-channel interference is very low. A heterogeneous population of user terminals with a large imbalance in the link quality is expected, as occurs when satellite resources are shared between large antenna fixed ground terminals and small antenna mobile platforms such as aircrafts. Single-antenna receivers are considered, with an arbitrary traffic demand across beams. The use of NOMA in DVB-S2X is evaluated for the forward link at the system level, using a new specific superframe profile, first presented in [3]. The exchange of resources across beams is also explored, in an effort to exploit NOMA to provide additional flexibility to resource allocation; under this beam-free approach, users can be paired across beam boundaries and served with NOMA, so traffic asymmetry in different beams can be leveraged to reap some benefits from a system perspective. This is expected to add on top of the advantages provided by NOMA when serving users with strong asymmetries in received SNR, due to the use of different front-ends. For completeness, non-linear impairments from the power amplification are also considered in the analysis, as they are expected to degrade the NOMA performance. In this paper, we will show how the operation point of the power amplifier should be jointly designed with NOMA power allocation to harness the potential NOMA improvement.

The rest of the paper is organized as follows. Section II presents the satellite system model. Next, the pairing of users and power allocation is addressed in Section III, whereas the effect of non-linearities is discussed in Section IV. Numerical results and conclusions are presented in Sections V and VI, respectively.

II. System Model

We consider a multibeam satellite system with M beams and K users across the coverage, with $K > M$. Conventional four-color frequency reuse across the beams is assumed, with the duration of the time-frequency resource slots equal to V. To evaluate the potential of the free scheduling of the users to the beams, we simplify the resource allocation process, and assume all available bandwidth W per beam is allocated to a single carrier. Consequently, the number of beams in the coverage sets the available frequency slots. The objective is to

carefully assign the users to the beam slots to optimize a given system metric in both OMA and NOMA cases, as showcased in Figure 1. The flexibility in the resource assignment is such that users can be freely served by any beam in the coverage. The received power from non-dominant beams is exploited, for example, by precoding schemes [8], [9], or to balance the traffic load of different beams [10]. Thus, resource allocation entails the user scheduling in both time and frequency dimensions, together with the optimization of the user rates. Finally, two terminals classes coexist on the satellite footprint, namely, strong and weak receivers, which have different front-ends[1], which give rise to a Signal-to-Interference and Noise Ratio (SINR) imbalance between them. In the case of NOMA, only two users will be served by each carrier at a given time instant, with Successive Interference Cancellation (SIC) performed only at the stronger receiver.

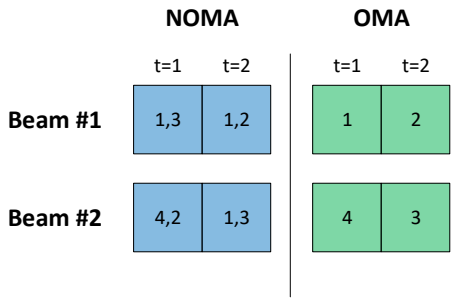

Fig. 1: Example of the flexible resource assignment. Each box displays the user indexes which are served by the corresponding beam.

We consider the application of the DVB-S2X standard. In the case of PD-NOMA, we employ the super-frame (SF) which is proposed in [3]. Under this SF profile, the generation of the corresponding NOMA-PLFRAME payload is depicted in Fig. 2, where the symbols of the combined DVB-S2X XFECFRAMEs (complex symbol frames) are aligned[2] and summed after being allocated a fraction of the total transmit power.

Furthermore, a non-linear power amplifier (PA) is considered for the evaluation of the spectral efficiency. For that purpose, let SINR_q^m denote the equivalent SINR of the q-th user when served by the m-th beam in a linear channel with the same PA output power as the saturation power P_{sat} in the non-linear case. With this notation, the corresponding achievable rates when the k-th and p-th users are allocated to the m-th beam in an orthogonal case can be written as

$$r_k^m = W \cdot \lambda_{kp}^m \cdot \Pi(\mathrm{SINR}_k^m, \mathrm{IBO}), \quad (1)$$

$$r_p^m = W \cdot (1 - \lambda_{kp}^m) \cdot \Pi(\mathrm{SINR}_p^m \mathrm{IBO}), \quad (2)$$

where W is the beam bandwidth, IBO is the Input Back-Off of the PA, Π is a mapping function for the DVB-S2X MODCODs, λ_{kp}^m and 1-λ_{kp}^m denote the slot time fraction to serve the k-th and the p-th users, respectively. Note that both SINR_k^m and IBO set the received power at the user terminal with a non-linear PA. In the case of NOMA, the rates are given by

$$\{r_k^m,\, r_p^m\} = W \cdot \Pi(\mathrm{SINR}_p^m, \mathrm{SINR}_k^m, \mathrm{IBO}, \lambda_{kp}^m) \quad (3)$$

where Π is a mapping function for the NOMA case that provides both the weak and strong spectral efficiencies with the DVB-S2X MODCODs, $\mathrm{SINR}_k^m > \mathrm{SINR}_p^m$, and λ_{kp}^m denotes the power fraction allocated to the kth user.

As a remark, let us mention that the allocation of a time-frequency resource provided by a given beam to an arbitrary user has practical limitations, since the user can be located so far away that the radiated power by the beam is not significant. We will exploit this to simplify the search for the optimal mapping between users and beams, with those on the first ring surrounding a central beam as potential candidates to serve the users located on the footprint of this central beam. For notation purposes, we define $\mathcal{S}^m$ as the set of users which can be served by the m-th beam, with size $|\mathcal{S}^m|$.

A. *Problem formulation*

With a fair sharing of resources in mind, we select proportional fair scheduling (PFS) to drive the resource allocation process with the beam free approach as in [11]; the PFS maximizes the geometric mean of the rates in the long run [12]. Under this policy, the long-term averaged rate of the user k with PFS is computed as

$$R_k(t+1) = \left(1 - \frac{1}{t_c}\right) r_k(t) + \frac{1}{t_c} r_k(t). \quad (4)$$

The instantaneous rate of the k-th user at time index t, $r_k(t)$, can be written as a function of the achievable rate by user k at time index t when served by the mth beam, $r_k^m(t)$:

$$r_k(t) = \sum_{m=1}^{M} u_k^m(t) r_k^m(t) \quad (5)$$

where $u_k^m(t)$ is a binary scheduling variable that is equal to 1 when the m-th beam serves the k-th user at time index t. With this notation, the PFS system metric for a given time slot can be reformulated as a weighted sum-rate (WSR) problem and expressed as

$$F(t) = \sum_{k=1}^{K} \frac{r_k(t)}{R_k(t)} \triangleq \sum_{k=1}^{K} w_k(t) r_k(t) \quad (6)$$

where $\{w_k(t)\}$ are the weights of the WSR problem, which are inversely proportional to the long-term rates. If the time

[1]For instance, due to different antenna sizes, or amplifiers with different noise figures.

[2]The superposition of strong and weak frames with possibly different modulations imposes some constraints on the combinations that can be accommodated, due to the different PLFRAME duration.

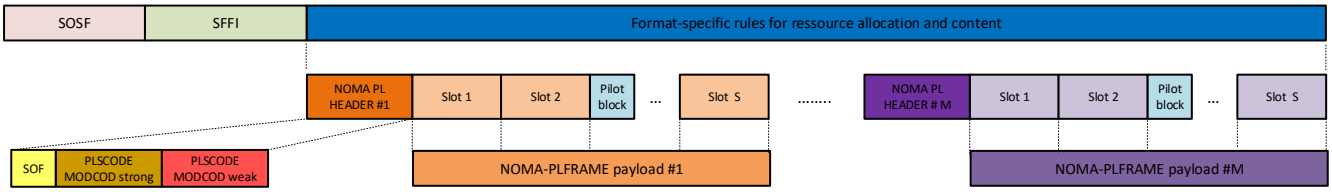

Fig. 2: Super-frame profile for PD-NOMA operation in DVB-S2X [3].

index is dropped to keep the notation simple, the resulting weighted sum-rate problem for the resource allocation can be expressed as

$$\max_{u_{kp}^m, \lambda_{kp}^m} \sum_{m=1}^{K} \sum_{k\in\mathcal{S}^m}^{|\mathcal{S}^m|} \sum_{p\in\mathcal{S}^m}^{|\mathcal{S}^m|} u_{kp}^m (w_k r_k^m + w_p r_p^m) \tag{7}$$

$$\text{s. to } u_{kp}^m \in \{0,1\}\ ; k,p \in \mathcal{S}^m$$

$$\text{A1}: \sum_{m=1}^{K} \sum_{k\in\mathcal{S}^m}^{|\mathcal{S}^m|} u_{kp}^m = 1\,, \forall p, m$$

$$\text{A2}: \sum_{m=1}^{K} \sum_{p\in\mathcal{S}^m}^{|\mathcal{S}^m|} u_{kp}^m = 1\,, \forall k, m$$

$$\text{A3}: \sum_{k\in\mathcal{S}^m}^{|\mathcal{S}^m|} \sum_{p\in\mathcal{S}^m}^{|\mathcal{S}^m|} u_{kp}^m = 1\,, \forall m$$

where u_{kp}^m is a scheduling variable that is active when both k-th and p-th users are paired and assigned to the m-th beam. The constraints A1, A2 and A3 ensure that users can only be served by one beam at a time, and each beam can only serve two users in a given time slot. The user scheduling u_{kp}^m, together with the rates r_k^m and r_p^m, will be driven by the maximization of WSR. Interestingly, the power per feed constraint allows us to decouple the problem in (7), and focus on the maximization of the user rates in each beam. For a given pair of users served by the mth beam, we can solve the following optimization problem

$$\max_{\lambda_{kp}^m} f(\lambda_{kp}^m) = w_k r_k^m + w_p r_p^m \tag{8}$$

$$\text{s. to } 0 \le \lambda_{kp}^m \le 1 \, \forall k, p \in \mathcal{S}^m$$

where the allocated fraction of resources λ_{kp}^m, either time (OMA) or power (NOMA), is omitted in the user rate description to keep the notation simple. With this, the optimization follows different paths for both OMA and NOMA, as detailed next:

- **OMA.**
  In the OMA case, the function $f(\lambda_{kp}^m)$ in (8) is monotonic with λ_{kp}^m. Therefore, one of the users will take the whole slot. With this, problem (7) boils down to a matching problem, which is expressed as

$$\max_{u_k} \sum_{m=1}^{K} \sum_{k\in\mathcal{S}^m}^{|\mathcal{S}^m|} u_k^m w_k r_k^m \tag{9}$$

$$\text{s. to } u_k^m \in \{0,1\}\ \forall\, k, m$$

$$\text{A1}: \sum_{m=1}^{K} u_k^m = 1\,, \forall k$$

$$\text{A2}: \sum_{k\in\mathcal{S}^m}^{|\mathcal{S}^m|} u_k^m = 1\,, \forall m.$$

  (A1) and (A2) ensure that a carrier beam is only allocated to one user at a time. The matching problem can be optimally solved by the Hungarian algorithm [13].
- **NOMA.** In the case of NOMA, the rates of the user pairs are obtained by selecting the best pair of DVB-S2X MDOCODs which optimize (8). On the other hand, the optimal user scheduling requires an exhaustive search exploring all possible solutions. As a practical implementation, an ad-hoc algorithm is presented in the next section.

III. Resource Allocation Algorithm for PD-NOMA

Since the maximization of the weighted sum-rate with NOMA signalling is known to be NP-hard [14], a heuristic algorithm has been developed to avoid an exhaustive search[3] . This algorithm is inspired by many-to-one matching theory [14], [15] and is outlined below. First, let be $\mathcal{C}^m$ a set of user indexes which indicates the candidates served by the m-th beam. This set will be labelled as a candidate set, and satisfies $\mathcal{C}^m \subset \mathcal{S}^m$. Under this notation, the weighted sum-rate of the candidates selected by the m-th beam can be expressed as WSR($\mathcal{C}^m$). Then, the overall weighted sum-rate of the system can be expressed as

$$U = \sum_{m=1}^{K} WSR(\mathcal{C}^m). \tag{10}$$

Furthermore, we consider single-carrier terminals, so that users can only be served by one beam at a time. To indicate this situation, we state a *user conflict* when two candidate sets intersect and aim to serve to the same user or group of users.

[3]This algorithm was included in the PhD thesis of the co-author Tomás Ramírez, and reproduced here for completeness.

For example, two candidate sets $\mathcal{C}^m$ and $\mathcal{C}^p$ present a user conflict if $\mathcal{A}^{m,p} = \mathcal{C}^m \cap \mathcal{C}^p$ and $|\mathcal{A}^{m,p}| \geq 1$, with $\mathcal{A}^{m,p}$ the set of user indexes from the user conflict. Thus, maximization of the metric in (10) consists of finding the adequate sets $\mathcal{C}^m$ without any user conflict. With this, the heuristic algorithm is split into two phases:

- **Initialization phase**: The algorithm starts by obtaining all possible pairs in $\mathcal{S}^m$ and maximizing the associated metric rate in (8), by selecting the best possible pair of DVB-S2X MODCODs. As a result of this initial phase, the results of pair-combination and weighted sum-rate are stored, and the highest WSR for each beam is attached to the corresponding candidate set $\mathcal{C}^m$.

- **Candidature approval phase**: If the proposed candidates $\{\mathcal{C}^m\}$ from the initialization phase do not pose any user conflict, then an optimal solution is achieved since each beam serves its best candidates. In general, guaranteeing the optimal solution is prohibitively expensive in terms of computational complexity. As a consequence, we resort to an ad-hoc algorithm with affordable cost, and without optimality guarantees, although the achieved solutions have been tested to be quite effective. In case of conflict, alternative candidate sets must be proposed, with the algorithm addressing two user candidate sets at a time. As a side effect, loops can appear in the algorithm, and further elaboration is needed. The detailed algorithm is presented in the Appendix.

IV. Non-Linear distortion

Due to limited available power in the satellite payload, the satellite channel usually presents a non-linear behavior due to distortion created by the power amplifiers (PA). This is due to the need of operating close to saturation to achieve acceptable onboard power efficiency. As the Input Back Off (IBO) reduces the non-linear distortion of the amplifier, we need to find a middle-ground between onboard power efficiency and non-linear distortion.

Non-linear effects are expected to be more detrimental for signals with higher dynamic range, which makes of special relevance to address their impact on PD-NOMA as the addition of two signals, in our case belonging to the family of DVB-S2X MODCODs. To this end, physical layer simulations have been performed for a hard-limiter TWTA model as in the DVB-S2X standard. This model, shown in Fig. 3, presents a linear region where the output back-off (OBO) equals the IBO values until the output power saturates.

The induced level of distortion is set by the PA operation point, through both P_{Sat} and IBO, and the Peak to Average Power Ratio (PAPR) of the input signal. In the case of super-imposed signals, the latter depends on the power allocation as presented in Fig 4. It is clear that the non-linear degradation, as an increasing function of PAPR, will vary with the relative contribution of each message to the NOMA signal.

Furthermore, each layer of the super-imposed signal can be affected differently by the non-linear distortion. For instance,

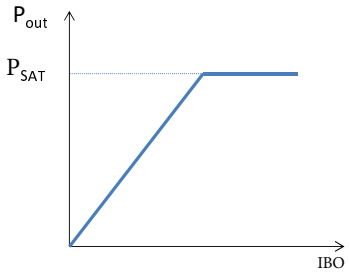

Fig. 3: Hard-limiter TWTA model [16].

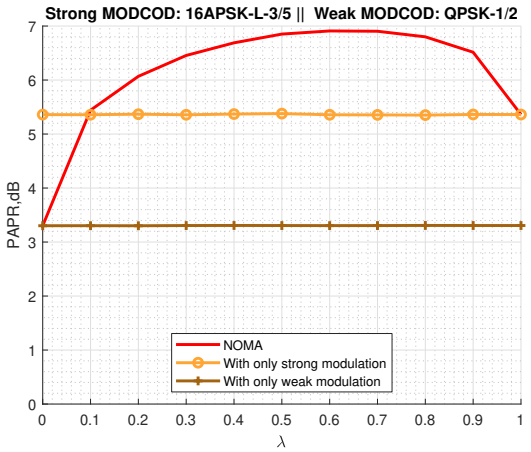

Fig. 4: PAPR values for the combination of two DVB-S2X MODCODs with respect to the power allocation of the strong message. 16-APSK-L-3/5 and QPSK-1/2 as the strong and weak MODCODs, respectively.

let us consider the reception of a NOMA signal, QPSK-modulated at each layer, under a linear and non-linear channel; the noiseless received signals are presented for both linear and non-linear PA at a strong receiver in Figure 5. By measuring the average Error Vector Magnitude (EVM) of the received signal with respect to an ideal reception for the different messages, we can observe the different degradation in each layer. In the case of the weak message, we obtain -5.6 dB for the linear case and -6.2 dB for the non-linear case. Note that the EVM is not null in the linear case, even in the absence of white noise, since the strong message is treated as additional noise. If the weak message is successfully suppressed in both linear and non-linear cases, the average EVM for the linear case becomes zero, whereas the non-linear cases provide an average EVM of -15.5 dB, since the non-linear components are not suppressed by the SIC process. As a consequence, **the power allocation λ in (9) must also be adjusted to compensate for the different signal degradation in each layer.**

A general procedure for the selection of the PA operation point, i.e., saturation power and IBO, is to minimize the required saturation power that results in successful demodulation of a selected MODCOD in the non-linear channel [17]. In

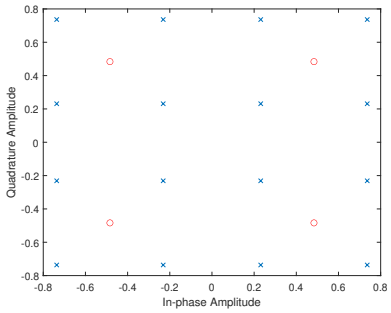

(a) Linear channel

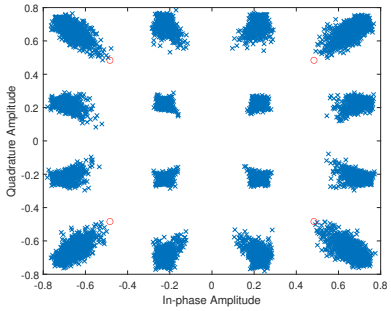

(b) Non-Linear channel

Fig. 5: PD-NOMA sample signals after the receiver matched filter with non-linear TWTA (hard limiter model). QPSK modulation is applied in each layer. Blue crosses represent the received symbols. Red circles represent the ideal received constellation.

addition, for the PD-NOMA case, the power allocation λ has also to be considered. Now, the goal is the joint selection of the PA operation point and power allocation λ to ensure a target frame error rate (FER) for both layered modulations. To this end, let Δ be the ratio between the required saturation power $\mathrm{P_{Sat}}$ in the non-linear channel and the transmission power $\mathrm{P_{Linear}}$ in a linear channel to achieve the target FER:

$$\Delta = \mathrm{P_{Sat}} - \mathrm{P_{Linear}} \quad \text{(dB)}. \tag{11}$$

Under this metric, the iterative method presented in Algorithm 1 describes the selection of the PA operation point and the power allocation λ. For illustration purposes, an example is depicted in Figure 6. Note that we can find an optimal value IBO that minimizes the required transmitted power. For high IBO values the non-linear distortion is negligible, and additional transmit power is needed to compensate for the SNR loss. As we move closer to saturation, the non-linear distortion grows, so that additional power is also required to compensate for the non-linear degradation. The physical layer simulations under this iterative approach have been performed with ideal time, frequency synchronization and SINR estimation. Although the non-linear effects could be reduced with the SIC process [18], only the linear components are suppressed and non-linear components are left as cancellation residue. Exhaustive simulations have been performed to minimize the required saturation power for different combinations of DVB-S2X MODCODs. An operation point is considered to be valid when the NOMA FECFRAME error is equal to or below 10^{-3} on average[4]. As evidence of the practical relevance of the described method, the growth of the NOMA rate region from the optimization of the power coefficient is presented in Fig. 7, as an example making use of DVB-S2X MODCODs. As we can observe, the joint optimization of IBO and power allocation λ can extend the achievable rates for the strong and weak users in the NOMA operation and increase the improvement over OMA.

Algorithm 1 Joint optimization of PA operation point and power allocation λ.

Input: Strong Message MODCOD, Weak Message MODCOD, Target FER, $\mathrm{P_{Lineal}}$, initial Input-Back Off value IBO^0, IBO search step μ_{IBO}.

Output: Saturation power P_{sat}, Input-Back Off IBO, power allocation λ.

1: Set input-back off to IBO^0.
2: Obtain values of P^0_{sat} and λ^0 to achieve the Target FER for both selected MODCODs.
3: Measure the additional power due to the non-linear degradation: $\Delta^0 = \mathrm{P}^0_{sat} - \mathrm{P_{Lineal}}$ dB.
4: $i = 1$.
5: **repeat**
6: Obtain values of P^i_{sat} and λ^i to achieve the Target FER for both selected MODCODs.
7: Measure the additional power due to the non-linear degradation: $\Delta^i = \mathrm{P}^i_{sat} - \mathrm{P_{Lineal}}$ dB.
8: $i = i + 1$.
9: Update the IBO value by a step μ_{IBO}: $\mathrm{IBO}^i = \mathrm{IBO}^{i-1} - \mu_{\mathrm{IBO}}$.
10: **until** $\Delta^{i-1} < \Delta^i$
11: $\mathrm{P}_{sat} \leftarrow \mathrm{P}^i_{sat}$
12: $\mathrm{IBO} \leftarrow \mathrm{IBO}^i$
13: $\lambda \leftarrow \lambda^i$

V. Numerical Results

The beam-free approach for both NOMA and OMA has been tested in a satellite scenario, with an antenna radiation pattern covering Europe with 200 beams, provided by the European Space Agency (ESA) [19]. To keep the complexity of the simulations manageable, a set of $M = 16$ beams at the center of the coverage is selected to serve $K = 320$ users. For simplicity, we assume the same statistical distribution of strong and weak users across the beams. To model the user distribution, we resort to the Dirichlet distribution $Dir(K, \alpha)$, with $\boldsymbol{\alpha} = [\alpha_1, \ldots, \alpha_M]$; the α_i parameters are chosen to shape the traffic demand across cells. In particular, we set $\alpha_i = 1,\ i = 1, \ldots, K$ so that we explore an homogeneous case where every possible distribution of users among beams

[4]The magnitude of the FECFRAME error has been selected to limit the simulation duration.

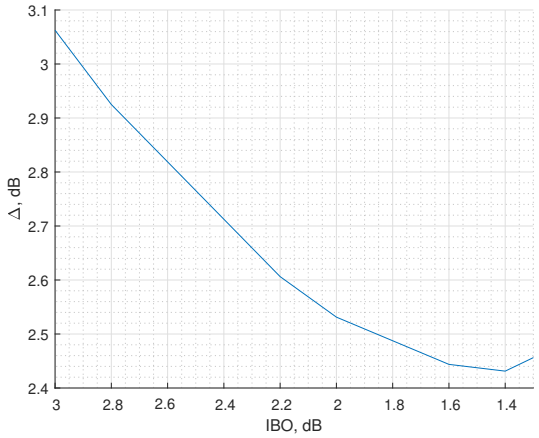

Fig. 6: Degradation due to non-linear operation with respect to IBO. MODCODs: QPSK 2/5 (weak), QPSK 5/6 (strong). SNR gap = 8 dB. FER= 10^{-3}.

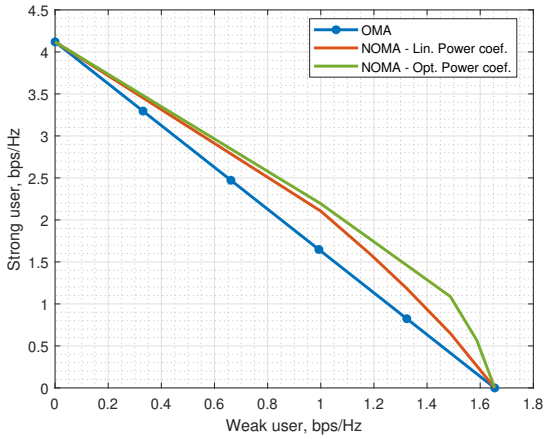

Fig. 7: NOMA rate region without (red) / with (green) joint optimization of the PA operation point and power allocation λ. SINR $=$ 17 dB for the strong user, and 10 dB power imbalance.

has equal probability. This will allow to obtain a general view of the potential performance with PD-NOMA. The number of transmission slots, V, has been set to 300 for both OMA and NOMA, high enough to include multiple transmissions for each user. The system parameters presented in Table I were used for the simulations, with 500 Monte-Carlo realizations. As mentioned in previous sections, the spectral efficiency will be measured for the DVB-S2X MODCODs taking into account the non-linear distortion of the PAs. The benchmarking metrics are the geometric mean, minimum rate and sum-rate, when comparing OMA and NOMA.

The overall system improvements of NOMA over OMA are presented for different ratios of strong and weak user per beam L in Fig. 8. Cumulative distribution functions of the total, strong and weak user rates, are also displayed in Figs. 9, 10 and 11, respectively. These average rates are computed

TABLE I: System parameters.

Satellite forward link	
Diagram pattern	Provided by ESA
Feed synchronisation	Perfect synchronisation
Number of beams	16
Number of feeds	16
Frequency band [GHz]	20
Total Bandwidth [MHz]	500
Beam Bandwidth [MHz]	250
EIRP/beam	68 dBW
Fading	Atmospheric losses
Common Receiver Parameters	
Receiver cloud noise temperature	280°K
Receiver terminal noise temperature	310°K
Receiver ground noise temperature	45°K
LNB Noise Figure	2 dB
Interference cancellation	Ideal cancellation
Strong Receiver Parameters	
Receiver antenna efficiency	0.65
Receiver antenna diameter	0.6 m
Weak Receiver Parameters	
Antenna gain gap to the strong receiver	10 dB

in each Monte-Carlo simulation, and measured as

$$\bar{r}_k = \frac{1}{V}\sum_{t=1}^{V} r_k(t), \tag{12}$$

where the variable $r_k(t)$ keeps track of the k-th user rate at the time slot t. From the results, NOMA clearly outperforms OMA in both geometric mean and sum-rate in Fig. 8. On the other side, Figs. 10 and 11 reveal that the NOMA gain applies mainly to strong users, for which the overall improvement on the average rate is around 30% (see Table II). Additionally, higher gains appear for higher L values, with more noticeable presence of strong users. There is a minor penalization for those weak users with lower rates, although the performance is quite aligned according to Fig. 11. With PD-NOMA, strong users can be served more frequently thanks to the non-orthogonal access, with a minimum impact to the service of weak users.

TABLE II: Average rate improvements of NOMA over OMA for weak and strong users.

	Weak users			Strong users		
Case	Geo.mean	Sum-Rate	Min.Rate	Geo.mean	Sum-Rate	Min.Rate
$L = 0.33$	-0.24 %	0.10 %	-2.32 %	26.39 %	27.35 %	30.99 %
$L = 1$	-0.50 %	0.30 %	-4.10 %	26.72 %	28.45 %	29.14 %
$L = 3$	-0.91 %	0.17 %	-6.01 %	27.26 %	29.66 %	27.72 %

VI. Conclusions

System level studies were presented for a multibeam scenario with different traffic demand patterns, where two different types of terminals coexisted, with a significant power imbalance in their respective link qualities. The potential gains of NOMA with respect to more conventional orthogonal allocation schemes were evaluated, after considering the use of specific DVB-S2X MODCODs, along with the impact of non-linearities, for which super-imposed signals are specially sensitive. The fair allocation of resources to the different

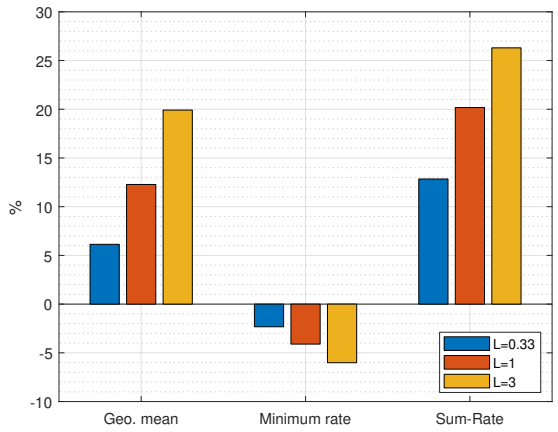

Fig. 8: Overall system improvement with PD-NOMA for homogeneous user distribution. L indicates the ratio between the number of strong and weak users within the beams.

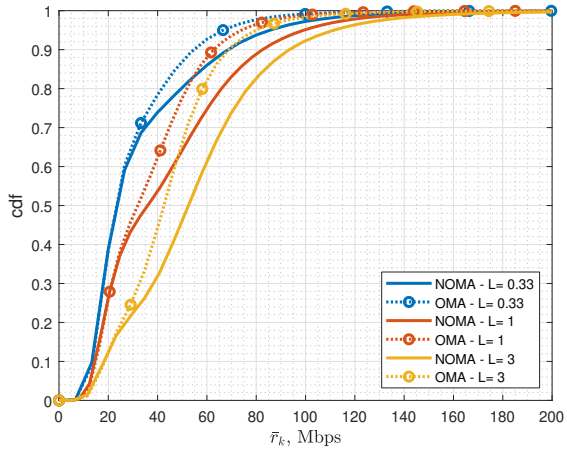

Fig. 9: Cumulative distribution of average user rates.

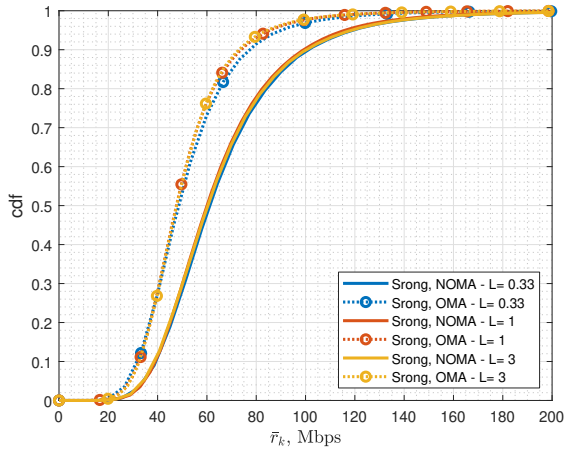

Fig. 10: Cumulative distribution of average strong user rates.

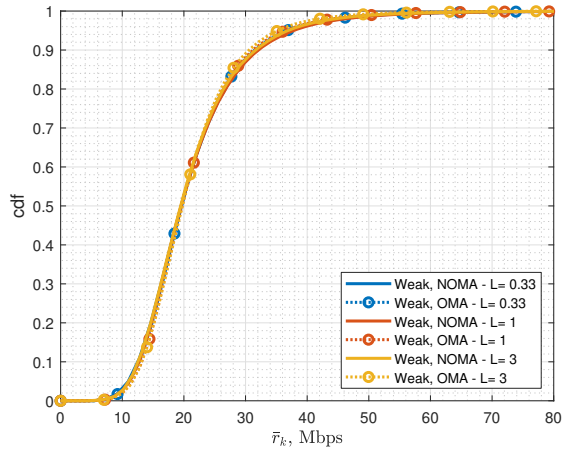

Fig. 11: Cumulative distribution of average weak user rates.

users across time was also embedded into the study. It was concluded that the power allocation in NOMA needs to be carefully optimized jointly with the input back-off of the power amplifiers to yield rate gains close to 30% for the strong users, while keeping similar overall rates for the weak users. Thus, NOMA appears as a candidate scheme to increase the provided throughput of a multibeam satellite, provided that at least the strong users are able to apply a SIC step.

ACKNOWLEDGMENT

Funded by MCIN/AEI/10.13039/501100011033/ FEDER and the European Union Next GenerationEU/PRTR, through the projects RODIN (PID2019-105717RB-C21) and REALSAT (PDC2021-120959-C22). Also funded by Xunta de Galicia (Secretaria Xeral de Universidades) under a predoctoral scholarship (cofunded by the European Social Fund).

APPENDIX

A. *User selection and pairing: conflict resolution*

Let $\mathcal{C}^m$ and $\mathcal{C}^p$ be two candidate sets that present a user conflict, with the users in conflict represented by a set $\mathcal{A}^{m,p}$. Furthermore, let us define $\mathcal{V}^m$ and $\mathcal{V}^p$ as alternative candidates that avoid any user conflict with $\mathcal{V}^m \cap \mathcal{P}^m \cap \mathcal{A}^{m,p} = \emptyset$ and $\mathcal{V}^p \cap \mathcal{P}^p \cap \mathcal{A}^{m,p} = \emptyset$. Here, $\mathcal{P}^m$ and $\mathcal{P}^p$ are a counter-measures to prevent loops; more details are given later. Under this formulation and taking into account the optimization metric of the algorithm, we also define

$$U_m = WSR(\mathcal{V}^m) + WSR(\mathcal{C}^p), \tag{13}$$

$$U_p = WSR(\mathcal{C}^m) + WSR(\mathcal{V}^p). \tag{14}$$

The user conflict resolution is dictated by comparing U_m and U_p. For instance, if $U_m \geq U_p$, the resolution goes in favor of the set $\mathcal{C}^p$ and the alternative set $\mathcal{V}^m$ becomes the new candidate set for the m-th beam. Moreover, the loop counter-measure $\mathcal{P}^m$ is updated as $\mathcal{P}^m = \mathcal{P}^m \cup \mathcal{A}^{m,p}$. Thus, this set keeps track of previous user conflicts and precludes forthcoming conflicts of the m-th beam with the already

resolved user conflict. In addition, the loop counter-measure $\mathcal{P}^p$ of the winner set is also updated by deleting the indexes of the conflicted users $\mathcal{A}^{m,p}$. If $U_m \leq U_p$ the same process applies in favor of the set $\mathcal{C}^m$.

As example, Figure 12 illustrates the process of user conflict resolution. Alternative sets are proposed after encountering a user conflict, which will be resolved in favor of one of the sets. Unfortunately, the ad-hoc algorithm does not guarantee an optimal solution and, in fact, candidate solutions with better performance than the final output of the algorithm might be discarded in the user conflict resolution process. As a consequence, the algorithm also stores the discarded solutions if they do not present any user conflict. The final achieved solution from the algorithm will be compared against the best solution across the discarded pool, and the best solution in terms of weighted sum-rate will be selected.

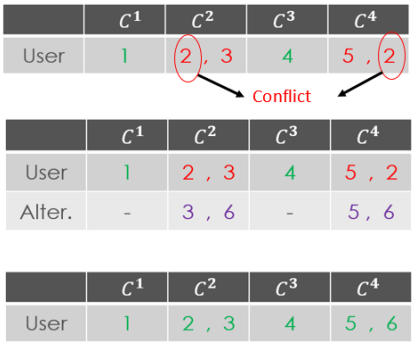

Fig. 12: Example of user conflict settlement.

REFERENCES

[1] Y. Saito, A. Benjebbour, Y. Kishiyama, and T. Nakamura, "System-level performance evaluation of downlink non-orthogonal multiple access (NOMA)," in *2013 IEEE 24th Annual International Symposium on Personal, Indoor, and Mobile Radio Communications (PIMRC)*. IEEE, 2013, pp. 611–615.

[2] N. Jindal, S. Vishwanath, and A. Goldsmith, "On the duality of Gaussian multiple-access and broadcast channels," *IEEE Trans. Inf. Theory*, vol. 50, no. 5, pp. 768–783, 2004.

[3] T. Ramírez, C. Mosquera, N. Noels, M. Caus, J. Bas, L. Blanco, and N. Alagha, "Study on the Application of NOMA Techniques for Heterogeneous Satellite Terminals," in *2020 10th Advanced Satellite Multimedia Systems Conference and the 16th Signal Processing for Space Communications Workshop (ASMS/SPSC)*, 2020, pp. 1–8.

[4] A. I. Perez-Neira, M. Caus, and M. A. Vazquez, "Non-orthogonal transmission techniques for multibeam satellite systems," *IEEE communications magazine*, vol. 57, no. 12, pp. 58–63, 2019.

[5] Y. Zhu, C. A. Hofmann, and A. Knopp, "Distributed Resource Optimization for NOMA Transmission in Beamforming SATCOM," *IEEE Journal on Selected Areas in Communications*, vol. 40, no. 4, pp. 1190–1209, 2022.

[6] L. Yin and B. Clerckx, "Rate-splitting multiple access for multigroup multicast and multibeam satellite systems," *IEEE Transactions on Communications*, vol. 69, no. 2, pp. 976–990, 2020.

[7] C. Mosquera, N. Noels, T. Ramírez, M. Caus, and A. Pastore, "Space-Time Rate Splitting for the MISO BC with Magnitude CSIT," *IEEE Transactions on Communications*, vol. 69, no. 7, pp. 4417–4432, 2021.

[8] M. Á. Vázquez, A. Perez-Neira, D. Christopoulos, S. Chatzinotas, B. Ottersten, P.-D. Arapoglou, A. Ginesi, and G. Taricco, "Precoding in multibeam satellite communications: Present and future challenges," *IEEE Wireless Communications*, vol. 23, no. 6, pp. 88–95, 2016.

[9] A. Guidotti and A. Vanelli-Coralli, "Clustering strategies for multicast precoding in multibeam satellite systems," *International Journal of Satellite Communications and Networking*, vol. 38, no. 2, pp. 85–104, 2020.

[10] T. Ramírez, C. Mosquera, and N. Alagha, "Flexible user mapping for radio resource assignment in advanced satellite payloads," *IEEE Transactions on Broadcasting*, 2022.

[11] T. Ramírez and C. Mosquera, "Resource Management in the Multibeam NOMA-based Satellite Downlink," in *IEEE International Conference on Acoustics, Speech and Signal Processing (ICASSP)*, 2020, pp. 8812–8816.

[12] Hoon Kim, Keunyoung Kim, Youngnam Han, and Sangboh Yun, "A proportional fair scheduling for multicarrier transmission systems," in *IEEE 60th Vehicular Technology Conference, 2004. VTC2004-Fall. 2004*, vol. 1, Sep. 2004, pp. 409–413 Vol. 1.

[13] H. W. Kuhn, "The Hungarian method for the assignment problem," *Naval Research Logistics Quarterly*, vol. 2, no. 1-2, pp. 83–97, 1955. [Online]. Available: https://onlinelibrary.wiley.com/doi/abs/10.1002/nav.3800020109

[14] B. Di, L. Song, and Y. Li, "Sub-Channel Assignment, Power Allocation, and User Scheduling for Non-Orthogonal Multiple Access Networks," *IEEE Transactions on Wireless Communications*, vol. 15, no. 11, pp. 7686–7698, Nov 2016.

[15] E. Bodine-Baron, C. Lee, A. Chong, B. Hassibi, and A. Wierman, "Peer Effects and Stability in Matching Markets," in *Algorithmic Game Theory*. Berlin, Heidelberg: Springer Berlin Heidelberg, 2011, pp. 117–129.

[16] ETSI, "Digital Video Broadcasting (DVB); Second generation framing structure, channel coding and modulation systems for Broadcasting, Interactive Services, News Gathering and other broadband satellite applications; Part II: S2- Extensions (S2-X)," European Standard (EN) EN 302 307-2, 2014.

[17] R. De Gaudenzi, A. Guillen i Fabregas, and A. Martinez, "Performance analysis of turbo-coded APSK modulations over nonlinear satellite channels," *IEEE Trans. Wireless Commun.*, vol. 5, no. 9, pp. 2396–2407, 2006.

[18] K. Kubo, S. Naoi, Y. Takeda, R. Miyamoto, T. Hara, and M. Okada, "Compensations of Nonlinear Effects of TWTA for Signal Super-Positioning Satellite Communication Systems," in *Personal Satellite Services*. Berlin, Heidelberg: Springer Berlin Heidelberg, 2010, pp. 44–59.

[19] R. De Gaudenzi, N. Alagha, M. Angelone, and G. Gallinaro, "Exploiting code division multiplexing with decentralized multiuser detection in the satellite multibeam forward link," *International Journal of Satellite Communications and Networking*, vol. 36, no. 3, pp. 239–276, 2018. [Online]. Available: https://onlinelibrary.wiley.com/doi/abs/10.1002/sat.1215